CMS Physics Analysis Summary

Contact: cms-pag-conveners-heavyions@cern.ch 2019/11/05

Measurement of the elliptic flow of Y(1S) and Y(2S) mesons in PbPb collisions at $\sqrt{s_{NN}} = 5.02$ TeV

The CMS Collaboration

Abstract

The second-order Fourier coefficients (v_2) characterizing the azimuthal dependence of Y(1S) and Y(2S) mesons arising from PbPb collisions at $\sqrt{s_{NN}} = 5.02$ TeV are determined. The Y mesons are reconstructed using the di-muon decay channel as measured using the CMS detector. The dataset was obtained in 2018 and corresponds to an integrated luminosity of 1.7 nb^{-1}. The scalar product method is used for the v_2 analysis. Results are reported for the rapidity range $|y| < 2.4$, with $0 < p_T < 50$ GeV, and in four centrality classes of 0-10%, 10-30%, 30-50% and 50-90%, with 0-10% corresponding to the most central collisions. The average v_2 value for Y(1S) mesons is 0.007 $\pm$ 0.011 (stat) $\pm$ 0.005 (syst) in the 10-90% centrality interval. The observed v_2 values are consistent with zero for all p_T and centrality ranges, with a maximum offset of 2.5 standard deviations. The v_2 value for Y(2S) mesons is measured for the first time and found to be -0.063 $\pm$ 0.085 (stat) $\pm$ 0.037 (syst) in the 10-90% centrality interval.

The primary motivation for studying high-energy heavy ion collisions is to better understand the hot and dense matter produced in these collisions. Lattice Quantum Chromodynamics calculations indicate that an environment is created where a crossover occurs from hadronic matter to a strongly interacting system of deconfined quarks and gluons [1], the so-called "quark-gluon plasma" (QGP) [2]. One of the most prominent signatures of QGP formation is the suppression of quarkonia, that is, the bound states of a heavy quark and its anti-quark, as the binding energy is weakened by the surrounding partons in the medium [3]. This suppression can be characterized in terms of the nuclear modification factor, R_{AA}, which is the ratio of the quarkonium yield in a nucleus-nucleus collision to the corresponding proton-proton (pp) yield at the same nucleon-nucleon center-of-mass energy, scaled by the number of binary collisions. Since the various quarkonia states have different binding energies, the extent of the screening is expected to reflect the given thermal environment, with the suppression pattern sequentially ordered by binding energy. For this reason, the bottomonia states (Y(1S), Y(2S), Y(3S), χ_b , etc.) are particularly interesting probes. A sequential suppression pattern was first observed for the Y(nS) mesons by the CMS experiment [4]. More recently, results with improved statistical precision have been reported by both the ALICE [5, 6] and CMS [7, 8] experiments. The suppression of Y(1S) meson has also been studied at the highest RHIC energy [9], and a measurement of Y(nS) suppression for all three states is planned at RHIC using the new sPHENIX detector [10]. The collective data, spanning from 200 GeV to 5.02 TeV, will provide new insight to the thermal properties of the QGP.

The R_{AA} studies, while sensitive to screening effects, are also affected by the nuclear parton distribution function (nPDF), which determines the quarkonia production rate. By studying the azimuthal dependence of the quarkonia particles, which is largely independent of the nPDF, it is possible to develop a more comprehensive understanding of the dynamics of quarkonia. The anisotropic distribution of particles in the transverse plane develops from the anisotropy of the overlap region of the colliding nuclei. The overlap in mid-central collisions is almond shaped and leads to an elliptic flow signal that can be characterized by the strength of the second-order Fourier coefficients (v_2) of the angular correlation of particles, with

$$\frac{dN}{d\phi} \propto 1 + 2\sum_n v_n \cos[n(\phi - \Psi_n)]. \tag{1}$$

Here ϕ is the azimuthal angle of particles and Ψ_n is the event plane angle of the n^{th} harmonic in the transverse plane [11].

Studies of the elliptic flow of light hadrons emitted in heavy ion collisions have provided significant information on the collective behavior of the QGP. Quarkonia can also develop a finite v_2 signal, and the elliptic flow of J/ψ mesons has been reported by both the ALICE [12, 13] and CMS [14, 15] Collaborations for both PbPb and pPb collisions. The ALICE collaboration has also measured the elliptic flow of Y(1S) mesons at forward rapidity using 5.02 TeV PbPb collisions [16]. In the case of bottomonia states, the flow signal is likely to originate from a path dependent suppression through Debye screening as the bottomonia traverses the medium. Bottom quarks are created by hard scatterings, before most of the soft particles that are produced at later stages of the collision. As such, there is little association between a heavy quark and the collective motion of the light quarks. Compared to J/ψ studies, one advantage of using Y mesons as a probe is that the contribution from late-stage recombination effects is smaller since the bottom quark is much heavier than the temperature scale of the QGP. This property allows bottomonia to better reflect the screening that occurs with passage through the QGP medium.

This note reports on the measurement of the second-order Fourier coefficient v_2 of Y(1S) and

Y(2S) mesons in PbPb collision at $\sqrt{s_{\mathrm{NN}}}$ = 5.02 TeV. The dataset was collected by the CMS detector in 2018 with an integrated luminosity of 1.7 nb^{-1}. The Y mesons are reconstructed using the dimuon decay channel. The v_2 coefficient is determined using the scalar-product method to obtain a root-mean-square v_2 value that is independent of the finite angular resolution of the reconstructed event plane [17], thus facilitating the comparison of theory calculations with the experimental results.

The central feature of the CMS apparatus is a superconducting solenoid of 6 m internal diameter, providing a magnetic field of 3.8 T. Within the solenoid volume are a silicon pixel and strip tracker, a lead tungstate crystal electromagnetic calorimeter (ECAL), and a brass and scintillator hadron calorimeter, each composed of a barrel and two endcap sections. Forward hadron (HF) calorimeters extend the pseudorapidity (η) coverage provided by the barrel and endcap detectors. Muons are detected in gas-ionization chambers embedded in the steel flux-return yoke outside the solenoid. A more detailed description of the CMS detector, together with a definition of the coordinate system used and the relevant kinematic variables, can be found in Ref. [18].

The dataset used in this analysis is for PbPb collisions at $\sqrt{s_{\mathrm{NN}}}$ = 5.02 TeV, taken in late 2018. Events were selected based on several layers of online triggers. First, at least two muon candidates reconstructed in the fast hardware-based trigger system (Level-1) are required. In the high level trigger (HLT), Level-2 (L2) muons are identified by requiring track fits in the outer muon spectrometer. At Level-3 (L3), muons are reconstructed using full tracks from the L2 muon tracks and the inner tracker information, with a minimum of 10 high-quality hits in the inner tracker [19]. Finally, events are required to contain one L2 muon and another L3 muon, with their invariant mass being greater than 7 GeV. To reject beam-related background processes (beam scraping events and beam-gas collisions), events are required to pass extra conditions: (a) that at least one reconstructed primary vertex exists, (b) that at least 25% of the tracks pass a tight track-quality selection [20], (c) that the width of silicon pixel detector clusters be compatible with the vertex position [21], and (d) that at least three towers in each of the two HF detectors located on opposite sides of CMS detect energy above 3 GeV. The primary vertex is required to be located within 15 cm from the central point of the detector along the beam axis.

For high quality muon identification, an offline selection criterium is also applied. This selection requires that the reconstructed muons be matched with an inner track, which has at least six silicon tracker hits, with at least one of these hits occurring in the inner silicon pixel array. In addition, the distance of a muon track from the nearest primary vertex must be less than 3 mm and 20 cm in the transverse and the longitudinal directions, respectively. To assure high efficiency, the individual muons were required to have $p_{\mathrm{T}}^{\mu} > 3.5$ GeV, with $|\eta^{\mu}| < 2.4$. Oppositely charged muon pairs are fitted with a common vertex constraint and used in this analysis if the fit χ^2 probability is larger than 1%.

The v_2 values for Y(1S) mesons are measured for $|y| < 2.4$, in four p_{T} bins (0–3 GeV, 3–6 GeV, 6–10 GeV, 10–50 GeV). Centrality is defined as the degree of overlap of the two colliding Pb nuclei and is estimated using the percentiles of the distribution of the sum of transverse energy deposited in the HF calorimeters. For this analysis, events are classified in four centrality intervals (0–10%, 10–30%, 30–50%, 50–90%), with 0–10% corresponding to the most central events. Because of the reduced yield of Y(2S) mesons, only the v_2 value with $|y| < 2.4$, $0 < p_{\mathrm{T}} < 50$ GeV, and 10–90% centrality is shown for this channel. For the p_{T} differential analysis, the 10–30% and 30–50% bins are merged. The peripheral collisions corresponding to the 90–100% centrality interval are excluded because of low event selection efficiency. The $\mathrm{Y} \to \mu^+\mu^-$ channel is used

for the mass identification. The Y signals and combinatorial backgrounds for selected dimuon pairs are separated using fits to the invariant mass distribution. The range of the studied mass spectrum is 8–14 GeV, which covers all Y(1S), Y(2S) and Y(3S) resonance peaks.

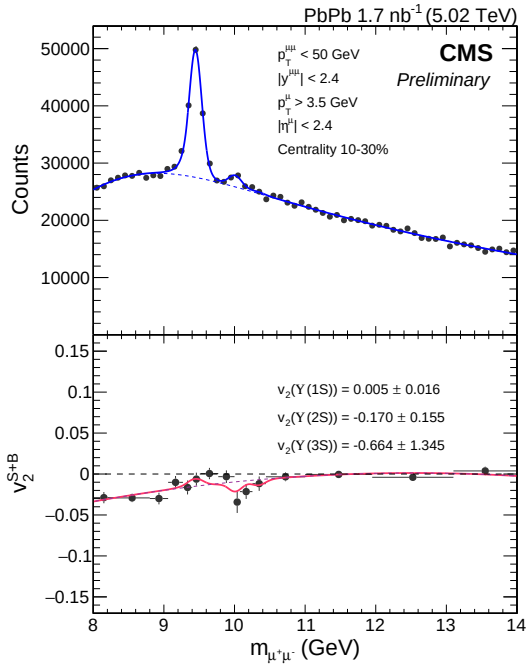

Figure 1: Simultaneous fit of the dimuon invariant mass spectrum and the ${v_2}^{S+B}$ distribution, as defined in Eq. 3, for $p_T < 50$ GeV and with centrality 10–30%. The solid (signal + background) and dashed (background only) blue lines show the result of the mass fit, and the solid and dashed red lines show the corresponding results for the fit to the v_2 distribution.

The reciprocals of the acceptance and efficiency correction factors are used as event-by-event weights when the invariant mass distribution and the average v_2 values are computed. Acceptance is defined as the probability for a Y meson to decay into the range of $p_T^{\mu} > 3.5$ GeV, $|\eta^{\mu}| < 2.4$. It is determined as a function of p_T using PYTHIA8 with CP5 tune [22], where Y mesons from ${}^3S_1$, ${}^3P_J$, ${}^3D_J$ bottomonium states form via the color-singlet and color-octet mechanisms. The MC events are then reweighted to match the p_T spectra to the PbPb data. The efficiencies for reconstruction, muon identification and trigger selection are calculated using a full simulation of the CMS detector using GEANT4 [23]. Each Y event is embedded in a HYDJET 1.9 [24] event to reproduce the hydrodynamic background environment. To account for the small difference found between the simulation and real data, a systematic uncertainty is assigned to the efficiency based on the difference found between the MC results and collision data using the tag-and-probe (T&P) method with single muons from J/ψ mesons decays [25]. The efficiency ratio of data over simulation is applied as a weight for the derivation of the final dimuon efficiency.

The v_2 values of Y candidates are determined using the scalar product (SP) method, which was previously used to determine the elliptic flow of prompt D^0 mesons in PbPb collisions [26]. Using this method, the event plane angles are characterized by Q-vectors that are determined for different ranges of pseudorapidity using either tracker or HF colorimeter data. The Q vectors are given by $Q_2 = \sum_{k=1}^{M} \omega_k e^{2i\phi_k}$, where the sum is over the multiplicity of particles for the tracker and the number of towers for the HF calorimeters, ϕ is the azimuthal angle of the particle or the tower, and ω is a weighting factor given by the transverse momentum of a par-

ticle in the tracker or the transverse energy deposited in a tower. In this analysis, three event plane Q-vectors are calculated from the tracker, with $|\eta| < 0.75$, and the two forward hadronic calorimeters, with $3 < \eta < 5$ (HF+) and $-5 < \eta < -3$ (HF-). The Q-vector of a Y candidate is defined as $Q_{2,\mathrm{Y}} = e^{i2\phi}$ where ϕ is the azimuthal angle of the candidate. The v_2 coefficient is then given by

$$v_2\{\mathrm{SP}\} \equiv \frac{\langle Q_{2,\mathrm{Y}} Q_{2A}^* \rangle}{\sqrt{\frac{\langle Q_{2A} Q_{2B}^* \rangle \langle Q_{2A} Q_{2C}^* \rangle}{\langle Q_{2B} Q_{2C}^* \rangle}}}, \tag{2}$$

where the subscripts A and B refer to either HF+ or HF- event plane, depending on the rapidity of the Y candidate. To avoid autocorrelations and to reduce nonflow effects, the η gap between Y candidates and the event plane detector is required to be at least 3 units. For this reason, HF+ is selected for the A (B) event plane when the Y candidate is produced at negative (positive) rapidity. The subscript C denotes the event plane obtained using tracker information. The $\langle\rangle$ brackets denote averages over all Y candidate events, taking the real part of the Q-vector products. The denominator in Eq. 2 accounts for finite resolution of the experimental event planes. The bottom panel of Fig. 1 shows an example of the resulting v_2 distribution as a function of the Y candidate invariant mass.

The separation of signal and background is done in two steps. First, the yields of Y signals are extracted from the invariant mass distribution without using the v_2 information. The purpose of this step is to find the best parameters for the probability distribution function (PDF) describing the Y peaks. The analysis is done using a single rapidity bin with $|y| < 2.4$ and, thus, uses Y candidates obtained in both the barrel and endcap regions of CMS. For this reason, the signal template for each Y meson is formed by the sum of two Crystal-Ball functions (CB) [27], to account for the different mass resolutions of the two regions. For both CB functions, the mass and the radiative-tail parameters are constrained to be equal since these are not sensitive to the detector resolution. The Y(1S) mass is taken as a free parameter, allowing for a possible scaling error in the momentum calibration for the reconstructed tracks. The mean (m_0) and width (σ) parameters for the excited states (Y(2S) and Y(3S)) are found by scaling the Y(1S) values by the ratio of published masses [28]. Other parameters for the excited states are constrained to be identical to those of the Y(1S) mesons. The normalization parameters $N_{sig,1S}$, $N_{sig,2S}$ and $N_{sig,3S}$ are allowed to be free parameters.

The PDF of the background mass is made by multiplying a real-valued error function and an exponential function. The error function is used to reproduce a kinematic enhancement found at low mass resulting from the single muon p_{T} threshold. The exponential component is motivated by the exponentially falling structure of the combinatorial background in the high mass region. There are four parameters characterizing the shape of the background, the μ and σ parameters of the the error function, the decay length of the exponential function, and an overall normalization parameter N_{bkg}. Unbinned log-likelihood fits to the mass distribution were used to obtain the best PDF fit to the data.

In the second step, the invariant mass distribution and v_2 profile are fitted simultaneously using binned chi-square fits. The previously obtained PDF parameters are used, although with the normalizations $N_{sig,1S}$, $N_{sig,2S}$ and $N_{sig,3S}$ allowed to vary. The v_2 dependence on m_{inv} is taken as

$$v_2^{Sig+Bkg}(m_{inv}) = \alpha_1(m_{\rm inv})v_2^{\Upsilon(1S)} + \alpha_2(m_{\rm inv})v_2^{\Upsilon(2S)} + \alpha_3(m_{\rm inv})v_2^{\Upsilon(3S)} + [1-\alpha_1(m_{\rm inv})-\alpha_2(m_{\rm inv})-\alpha_3(m_{\rm inv})]v_2^{Bkg}(m_{\rm inv}), \quad (3)$$

where

$$\alpha_i(m_{inv}) = Sig_{\Upsilon(iS)}/(Sig_{\Upsilon(1S)}(m_{\rm inv}) + Sig_{\Upsilon(2S)}(m_{\rm inv}) + Sig_{\Upsilon(3S)}(m_{\rm inv}) + Bkg(m_{\rm inv})). \quad (4)$$

Here, $v_2^{\Upsilon(iS)}$ is the v_2 value for the Y(iS) mesons and is assumed to be independent of m_{inv}. The $\alpha_i(m_{\rm inv})$ coefficients are the fractions that the Y(iS) states occupy as a function of invariant mass, as determined by the mass fit. The background v_2 value, $v_2^{Bkg}(m_{\rm inv})$, is modeled as a second order polynomial function of the invariant mass. Fig. 1 shows an example of a simultaneous fit to the mass distribution (top) and v_2 profile (bottom).

The systematic uncertainties in this analysis come from various sources, including the modeling of signal and background PDF and the acceptance and efficiency corrections (muon ID and trigger). For the uncertainty associated with the signal PDF, an alternative PDF is formed by adding one Crystal-Ball function and one Gaussian function. The difference in the new v_2 value from the nominal one is taken as the uncertainty. The uncertainties resulting from holding final fit parameters constant are studied by releasing each parameter, one by one, and redoing the fit with the additional free parameter. The largest deviation of the resulting v_2 values from the nominal result is taken as the uncertainty. To determine the uncertainty in the background PDF, the PDF's for both the invariant mass distribution and $v_2^{Bkg}(m_{\rm inv})$ were varied. For the mass distribution, a fourth-order polynomial is used as an alternative functional behavior. For the $v_2^{Bkg}(m_{\rm inv})$ PDF, a third-order polynomial function is used instead of the nominal second-order polynomial. The deviation of the final result with each alteration is taken as the associated systematic uncertainty. The uncertainty resulting from the acceptance correction is evaluated by comparing the result with and without applying correction factors. By virtue of the cylindrical symmetry of the detector, the effects of this correction are small. The effect of the efficiency uncertainty is based on the difference found between the MC derived efficiency values to those obtained using the tag-and-probe (T&P) method. Finally, uncertainties resulting from the hadronic event selection are considered. The collision event filter is varied, thus allowing for a migration of Y(1S) mesons across centrality boundaries. The effect on the deduced v_2 values is taken as a systematic uncertainty. The individual systematic uncertainties are expected to be uncorrelated and are therefore added in quadrature for the final quoted values. The absolute systematic uncertainty on the v_2 values for the Y(1S) meson range from 0.002 to 0.026, with the largest uncertainty corresponding to the most peripheral and lowest $p_{\rm T}$ interval measured.

The $p_{\rm T}$ integrated results are shown in the left-hand side of Fig. 2 for four centrality intervals. The Y(1S) v_2 values are consistent with zero within the statistical uncertainties, with a maximum statistical deviation of $\approx 1\sigma$ being found for the 30–50% centrality interval. The right most points in this figure are the average v_2 values in the 10–90% centrality interval. They are determined to be 0.007 $\pm$ 0.011 (stat) $\pm$ 0.005 (syst) for Y(1S) mesons and -0.063 $\pm$ 0.085 (stat) $\pm$ 0.037 (syst) for Y(2S) mesons. Despite the large number of produced Y(1S) mesons, the statistical uncertainty in the most central bin is larger than in other centrality ranges because the term in the numerator in Eq. 2, $\langle Q_{2,\Upsilon}, Q_A^* \rangle$, has a smaller amplitude. This observation can be explained by a circular shape of the collision geometry in the transverse plane for central

events leading to a small v_2 azimuthal asymmetry in the region used to determine the event plane angle. Since it does not have a significant influence on the centrality integrated results, the 0–10% bin is excluded in determining the centrality integrated results.

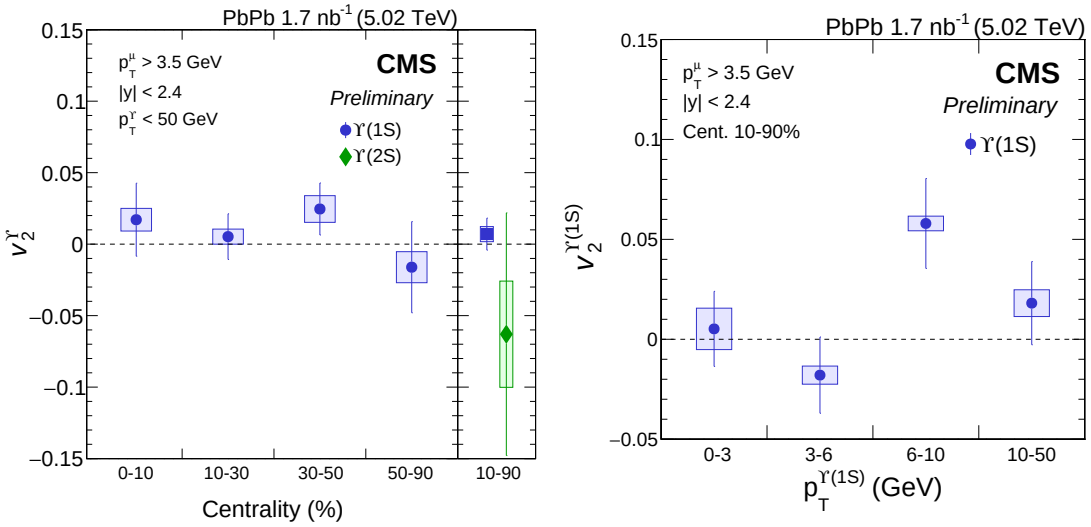

Figure 2: (Left) p_{T} integrated v_2 values for Y(1S) mesons measured in four centrality bins and for the Y(2S) meson in the 10–90% centrality range. (Right) v_2 as a function of p_{T} in the 10–90% centrality range. All results are for the rapidity range of $|y| < 2.4$. The vertical bars denote statistical uncertainties, and the rectangular bands show the total systematic uncertainties.

On the right-hand side of Fig. 2, the p_{T} dependence of Y(1S) v_2 values is shown for the 10–90% interval. The result is observed to be consistent with zero for all bins, except for the $6 < p_{\mathrm{T}} < 10$ GeV range where the result is 2.5σ above zero when the systematic and statistical uncertainties are combined in quadrature. In Fig. 3 the measured Y(1S) results are compared with model calculations from Du and Rapp [29], from Hong and Lee [31], and from Yao [30].

The p_{T} differential results for Y(1S) mesons in each centrality bin are shown in Fig. 4. In the 0–10% bin, all v_2 values are consistent with zero within uncertainties, as expected. In the 10–50% interval, the v_2 value is generally consistent with zero except for $6 < p_{\mathrm{T}} < 10$ GeV, which indicates a non-zero signal beyond the uncertainty. In the most peripheral bin, all v_2 results are consistent with zero within uncertainties.

In summary, the elliptic flow coefficient v_2 for Y(1S) and Y(2S) mesons are measured for $|y| < 2.4$ in PbPb collision at $\sqrt{s_{\mathrm{NN}}} = 5.02$ TeV. Results are reported for the rapidity range $|y| < 2.4$, with $0 < p_{\mathrm{T}} < 50$ GeV, and in four centrality classes of 0-10%, 10-30%, 30-50% and 50-90%, with 0-10% corresponding to the most central collisions. The v_2 values found for Y(1S) mesons are consistent with zero over the kinematic range studied, within a maximum of 2.5 standard deviations. This observation contrasts with the measured J/ψ v_2 results in PbPb collisions [13, 14], suggesting different medium effects for charmonia and bottomonia. The data are compared to several theoretical models, all consistent with the results. In addition the first measurement of the elliptic flow coefficient for Y(2S) mesons in a heavy ion experiment is also reported and the result is consistent with zero. Because the contribution of regeneration to Y(2S) meson production in PbPb collisions is expected to be different from that of Y(1S) meson and to occur at a later stage of the collision, this study provides new inputs to the production mechanisms of bottomonia in heavy ion collisions.

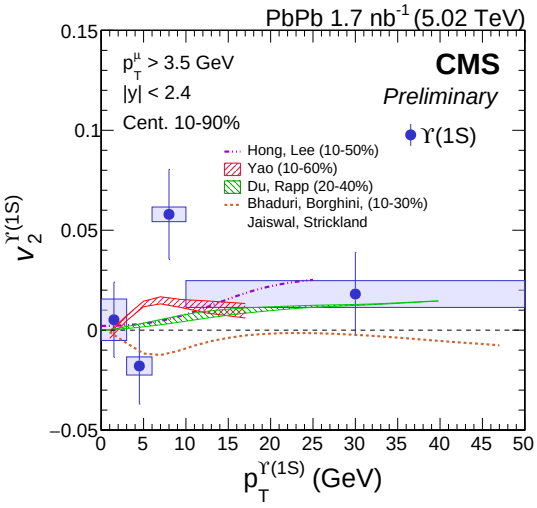

Figure 3: The green shaded area (Du, Rapp [29]) shows the results of a model calculation using the kinetic-rate equation to simulate the time evolution of bottom quarks. In this model, the medium effect is applied with a lattice-QCD based equation of state. The red band (Yao [30]) is the result of a real-time simulation of heavy quarks using coupled Boltzmann transport equations. The dashed violet line (Hong, Lee [31]) is the calculation with the potential Non-Relativistic QCD (pNRQCD) theory. In this approach, a diffusion constant D(2πT)=6 was used to have the derived R_{AA} value being consistent with the CMS result in Ref. [8]. The dashed brown line (Bhaduri, Borghini, Jaiswal, Strickland [32]) shows the results of using a 3+1d aHydro model. The calculations provide the QGP temperature evolution with the initial conditions and shear viscosity to entropy density ratio tuned to LHC 5.02 TeV identified hadron spectra and flow harmonics.

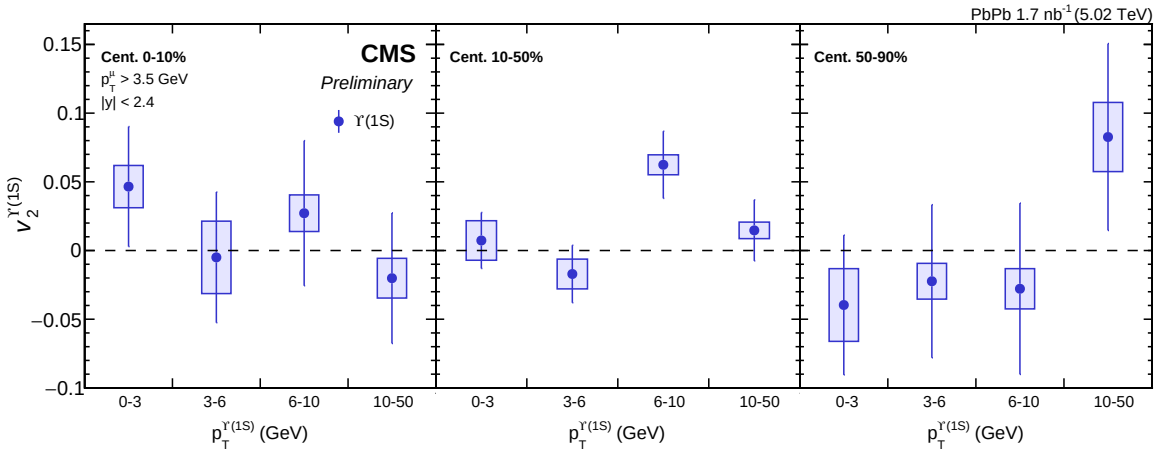

Figure 4: v_2 coefficients for Υ(1S) mesons as a function of p_T in three centrality bins: 0–10% (Left), 10–50% (Middle) and 50–90% (Right). The rapidity range is $|y| < 2.4$. The vertical lines indicate the statistical uncertainties and the rectangular bands show the total systematic uncertainties.

References

[1] F. Karsch, E. Laermann, and A. Peikert, "The Pressure in two flavor, (2+1)-flavor and three flavor QCD", *Phys. Lett. B* **478** (2000) 447–455, doi:10.1016/S0370-2693(00)00292-6, arXiv:hep-lat/0002003.

[2] E. V. Shuryak, "Theory of Hadronic Plasma", *Sov. Phys. JETP* **47** (1978) 212–219. [Zh. Eksp. Teor. Fiz.74,408(1978)].

[3] T. Matsui and H. Satz, "J/ψ Suppression by Quark-Gluon Plasma Formation", *Phys. Lett. B* **178** (1986) 416–422, doi:10.1016/0370-2693(86)91404-8.

[4] CMS Collaboration, "Suppression of $\Upsilon(1S)$, $\Upsilon(2S)$ and $\Upsilon(3S)$ production in PbPb collisions at $\sqrt{s_{\mathrm{NN}}}$ = 2.76 TeV", *Phys. Lett. B* **770** (2017) 357–379, doi:10.1016/j.physletb.2017.04.031, arXiv:1611.01510.

[5] ALICE Collaboration, "Suppression of $\Upsilon(1S)$ at forward rapidity in Pb-Pb collisions at $\sqrt{s_{\mathrm{NN}}} = 2.76$ TeV", *Phys. Lett. B* **738** (2014) 361–372, doi:10.1016/j.physletb.2014.10.001, arXiv:1405.4493.

[6] ALICE Collaboration, "Y suppression at forward rapidity in Pb-Pb collisions at $\sqrt{s_{\mathrm{NN}}}$ = 5.02 TeV", *Phys. Lett. B* **790** (2019) 89–101, doi:10.1016/j.physletb.2018.11.067, arXiv:1805.04387.

[7] CMS Collaboration, "Suppression of Excited Y States Relative to the Ground State in Pb-Pb Collisions at $\sqrt{s_{\mathrm{NN}}}$=5.02 TeV", *Phys. Rev. Lett.* **120** (2018), no. 14, 142301, doi:10.1103/PhysRevLett.120.142301, arXiv:1706.05984.

[8] CMS Collaboration, "Measurement of nuclear modification factors of Y(1S), Y(2S), and Y(3S) mesons in PbPb collisions at $\sqrt{s_{\mathrm{NN}}} = 5.02$ TeV", *Phys. Lett. B* **790** (2019) 270–293, doi:10.1016/j.physletb.2019.01.006, arXiv:1805.09215.

[9] STAR Collaboration, "Suppression of Y production in d+Au and Au+Au collisions at $\sqrt{s_{NN}}$=200 GeV", *Phys. Lett. B* **735** (2014) 127–137, doi:10.1016/j.physletb.2014.06.028, 10.1016/j.physletb.2015.01.046, arXiv:1312.3675. [Erratum: Phys. Lett.B 743,537(2015)].

[10] PHENIX Collaboration, "An Upgrade Proposal from the PHENIX Collaboration", arXiv:1501.06197.

[11] S. Voloshin and Y. Zhang, "Flow study in relativistic nuclear collisions by Fourier expansion of Azimuthal particle distributions", *Z. Phys. C* **70** (1996) 665–672, doi:10.1007/s002880050141, arXiv:hep-ph/9407282.

[12] ALICE Collaboration, "Search for collectivity with azimuthal J/ψ-hadrons in high-multiplicity p-Pb collisions at $\sqrt{s_{\mathrm{NN}}} = 5.02$ TeV and 8.16 TeV", *Phys. Lett. B* **780** (2018) 7, doi:10.1016/j.physletb.2018.02.039, arXiv:1709.06807.

[13] ALICE Collaboration, "J/ψ Elliptic Flow in Pb-Pb Collisions at $\sqrt{s_{NN}} = 5.02$ TeV", *Phys. Rev. Lett.* **119** (2017) 242301, doi:10.1103/PhysRevLett.119.242301, arXiv:1709.05260.

[14] CMS Collaboration, "Suppression and azimuthal anisotropy of prompt and nonprompt J/ψ production in PbPb collisions at $\sqrt{s_{\mathrm{NN}}} = 2.76$ TeV", *Eur. Phys. J. C* **77** (2017) 252, doi:10.1140/epjc/s10052-017-4781-1, arXiv:1610.00613.

[15] CMS Collaboration, "Observation of prompt J/ψ meson elliptic flow in high-multiplicity pPb collisions at $\sqrt{s_{\mathrm{NN}}} = 8.16$ TeV", *Phys. Lett. B* **791** (2019) 172–194, doi:10.1016/j.physletb.2019.02.018, arXiv:1810.01473.

[16] ALICE Collaboration, "Measurement of $\Upsilon(1S)$ elliptic flow at forward rapidity in Pb-Pb collisions at $\sqrt{s_{\mathrm{NN}}} = 5.02$ TeV", arXiv:1907.03169.

[17] M. Luzum and J.-Y. Ollitrault, "Eliminating experimental bias in anisotropic-flow measurements of high-energy nuclear collisions", *Phys. Rev. C* **87** (2013) 044907, doi:10.1103/PhysRevC.87.044907.

[18] CMS Collaboration, "The CMS experiment at the CERN LHC", *JINST* **3** (2008) S08004, doi:10.1088/1748-0221/3/08/S08004.

[19] CMS Collaboration, "The CMS trigger system", *JINST* **12** (2017) P01020, doi:10.1088/1748-0221/12/01/P01020.

[20] CMS Collaboration, "Description and performance of track and primary-vertex reconstruction with the CMS tracker", *JINST* **9** (2014) P10009, doi:10.1088/1748-0221/9/10/P10009, arXiv:1405.6569.

[21] CMS Collaboration, "Transverse momentum and pseudorapidity distributions of charged hadrons in pp collisions at $\sqrt{s} = 0.9$ and 2.36 TeV", *JHEP* **02** (2010) 041, doi:10.1007/JHEP02(2010)041, arXiv:1002.0621.

[22] T. Sjöstrand, S. Mrenna, and P. Skands, "PYTHIA 6.4 physics and manual", *JHEP* **05** (2006) 026, doi:10.1088/1126-6708/2006/05/026, arXiv:hep-ph/0603175.

[23] GEANT4 Collaboration, "GEANT4: A Simulation toolkit", *Nucl. Instrum. Meth. A* **506** (2003) 250–303, doi:10.1016/S0168-9002(03)01368-8.

[24] I. P. Lokhtin et al., "Heavy ion event generator HYDJET++ (HYDrodynamics plus JETs)", *Comput. Phys. Commun.* **180** (2009) 779–799, doi:10.1016/j.cpc.2008.11.015, arXiv:0809.2708.

[25] CMS Collaboration, "Performance of CMS Muon Reconstruction in pp Collision Events at $\sqrt{s} = 7$ TeV", *JINST* **7** (2012) P10002, doi:10.1088/1748-0221/7/10/P10002, arXiv:1206.4071.

[26] CMS Collaboration, "Measurement of prompt D^0 meson azimuthal anisotropy in Pb-Pb collisions at $\sqrt{s_{NN}} = 5.02$ TeV", *Phys. Rev. Lett.* **120** (2018), no. 20, 202301, doi:10.1103/PhysRevLett.120.202301, arXiv:1708.03497.

[27] M. Oreglia, "A Study of the Reactions $\psi' \to \gamma\gamma\psi$". PhD thesis, SLAC, 1980.

[28] Particle Data Group Collaboration, "Review of Particle Physics", *Chin. Phys. C* **40** (2016), no. 10, 100001, doi:10.1088/1674-1137/40/10/100001.

[29] X. Du, R. Rapp, and M. He, "Color Screening and Regeneration of Bottomonia in High-Energy Heavy-Ion Collisions", *Phys. Rev.* **C96** (2017), no. 5, 054901, doi:10.1103/PhysRevC.96.054901, arXiv:1706.08670.

[30] X. Yao et al., "Quarkonium production in heavy ion collisions: coupled Boltzmann transport equations", *PoS* **HardProbes2018** (2018) 157, doi:10.22323/1.345.0157, arXiv:1812.02238.

[31] J. Hong and S. H. Lee, "$\Upsilon(1S)$ transverse momentum spectra through dissociation and regeneration in heavy ion collisions", arXiv:1909.07696.

[32] P. P. Bhaduri, N. Borghini, A. Jaiswal, and M. Strickland, "Anisotropic escape mechanism and elliptic flow of bottomonia", arXiv:1809.06235.